



# Optimization of the femtosecond laser trepan drilling strategy on IN792 for improving hole geometrical characteristics and machining efficiency

Fengyun Zhang<sup>1,2,3</sup> · Shufeng Sun<sup>2,3</sup> · Xi Wang<sup>2</sup> · Jin Wang<sup>2</sup> · Yong Pang<sup>2</sup> · Jing Shao<sup>2</sup> · Jian Zhan<sup>2,4</sup>

Received: 14 November 2022 / Accepted: 4 May 2023 / Published online: 9 May 2023  
© The Author(s), under exclusive licence to Springer-Verlag London Ltd., part of Springer Nature 2023

## Abstract

Drilling film cooling holes (FCHs) that meet the stringent quality standards was a challenging task in aeroengine component manufacturing. This study aims to enhance the geometrical quality characteristics, such as hole taper and circularity, in the course of laser trepan drilling (LTD) of a 0.68-mm-thick IN792 superalloy while maintaining high processing efficiency and laser utilization. The linear correlation between the number of feeding times and entrance diameter has been confirmed, indicating that the diameter increases proportionally with the feeding times. This provides a useful reference for precise control of hole drilling geometry. By optimizing the scanning path and appropriately reducing the number of nested circles, machining efficiency improved. In addition, a variety of hybrid optimization strategies have revealed that moderately increasing the number of single-layer scanning times and adjusting the number of feeding times are key factors in establishing a suitable hole reaming process to improve machining quality and precisely control geometry. Finally, EDS analysis proved that only a small amount of oxygen was enriched at the orifice after removing oxides via oxidative ablation. Additionally, there were no heat-affected zones, oxidation zones, or recast layers.

**Keywords** Femtosecond laser · Trepan drilling · IN792 · Geometrical quality · Machining efficiency

## 1 Introduction

Laser machining has been favoured in several industries, viz., medical, chemical, automobile and aerospace industries, due to many advantages, such as a highly precise machining rate, high flexibility, repeatability and high operation speed

[1–5]. Laser drilling has been widely adopted in the aerospace industry and is currently an established technology for manufacturing film cooling holes (FCHs) in aeroengine blades and nozzle guide vanes due to its capability to drill difficult materials, such as superalloys and ceramics [6–8].

The FCH diameter is generally 0.1–1.25 mm, the hole diameter tolerance is 0.1 mm, the position tolerance is 0.1 to 0.15 mm, and the recast layer thickness is less than 0.02 mm [9]. The common processing strategies used for hole drilling include laser percussion drilling (LPD) and laser trepan drilling (LTD). In LPD, laser pulses are repeatedly delivered at a single point to produce a hole, and the hole size is changed with the input power and focusing adjustments. Nevertheless, large or noncircular holes, such as FCHs, are usually drilled by LTD, and the holes are cut by moving the workpiece or moving the laser beam. In LTD, the work material is targeted by a high-intensity laser beam with a microbeam spot, contributing to more than high power density or heat flux that can melt and/or vaporise all the targets [10, 11]. The advantage of LPD over LTD is the reduction in processing time, while the latter has the benefit of less amount of spatter and the thickness of the recast.

✉ Fengyun Zhang  
900fengyun@163.com

✉ Shufeng Sun  
sunshufeng@qut.edu.cn

<sup>1</sup> Key Lab of Industrial Fluid Energy Conservation and Pollution Control, (Qingdao University of Technology), Ministry of Education, Qingdao 266525, China

<sup>2</sup> Shandong Collaborative Innovation Center of Laser Green Intelligent Manufacturing Technology and Equipment, Qingdao University of Technology, Qingdao 266525, China

<sup>3</sup> School of Mechanical and Automotive Engineering, Qingdao University of Technology, 777 Jialingjiang Road, West Coast New Area, Qingdao 266525, China

<sup>4</sup> College of Mechanical & Electrical Engineering, Wenzhou University, Wenzhou 325035, China

In the laser drilling of FCHs, high precision, high quality and high efficiency have always been the three major problems to be solved; nevertheless, quality always conflicts with the processing efficiency. Traditional long-pulsed laser systems (milliseconds and nanoseconds) can always generate high ablation rates but induce defects, such as tapers, spatter deposition, recast layers and HAZ, which results in unreliable quality and reduced accuracy [12]. Instead, ultrashort pulse laser systems (picosecond or femtosecond) can improve the hole-drilling quality for the extremely short, intensive laser pulses and fast interaction between the laser beam and the material [13]. Under optimal conditions, ultrashort pulse laser ablation is not associated with residual melting and thus exhibits a clean finish. However, the material removal rate is low and in the range of 10–200 nm per laser pulse [7, 14]. In contrast, the material removal rate of millisecond laser drilling can exceed 1 mm and even 2 mm per laser pulse, which can be in the range of approximately  $10^3$ – $10^5$  times the ultrafast laser drilling efficiency [15, 16]. Due to the high machining precision requirements of FCHs, the thermal effect cannot be effectively constrained with traditional long-pulsed laser systems. Therefore, the current issue and challenge consists of effectively improving the processing efficiency of ultrashort pulse laser systems while ensuring machining precision and quality to meet the need and requirements for industrial applications [17].

LTD is progressively becoming the choice for precision drilling, but it has certain disadvantages, such as its high machining cost in the course of the process [18]. Several approaches have been implemented to improve the efficiency and precision of LTD, such as multistep machining strategies and dual-beam laser micromachining systems with different pulse lasers. Combining the advantages of traditional laser systems with ultrashort laser systems, Wang et al. [12] proposed a two-step drilling method on thermal barrier-coated nickel base alloys. Specifically, through holes were initially fabricated by a millisecond laser and subsequently refined by a femtosecond laser, and finally, drilled holes of high quality were obtained. Lin et al. [19] developed a dual-beam laser micromachining system consisting of a femtosecond laser and a nanosecond laser to enhance the ablation efficiency. Experiments were conducted in different materials, including dielectrics, semiconductors and metals. The material removal efficiency was found to increase in the dual-beam process for all materials being studied compared to a femtosecond laser or a nanosecond laser alone, particularly for dielectrics. Ito et al. [20] demonstrated the ultrafast precision drilling of glass by coaxially focusing a single femtosecond laser pulse and a fibre laser pulse, and the drilling speed was 5000 times faster than that of conventional femtosecond laser drilling. Jia et al. [21, 22] used a combined pulse laser (CPL) method for drilling alumina ceramic with an initial nanosecond pulse train that first irradiated the sample,

followed by a millisecond pulse train irradiated at the same position with a certain delay. Experimental results demonstrate the pretreatment of the initial nanosecond pulses could strengthen the performance of the subsequent millisecond pulses to diminish the diameter and cracks of the hole. Qin et al. [23] studied the principle of material removal and the process of hole formation during drilling with combined millisecond and nanosecond laser pulses, and the drilling efficiency was improved by the CPL method. The dual-beam system and multipulse combined laser-machining system can improve the quality and efficiency of hole machining, but they will produce secondary machining errors, which does not meet the required high-efficiency and high-precision machining of FCHs. Similar to laser-composite processing with different pulse widths, other processing methods can also be reasonably combined to achieve high-quality FCH processing while capitalizing on their respective advantages, such as laser-based hybrid/cross/assisted drilling techniques [5, 24, 25], as shown in Table 1.

For the microhole processing of different materials, the detailed information of some studies is shown in Table 1. Among existing laser hybrid drilling methods, the assistance strategies include ultrasound, multienergy fields, electrochemistry/chemistry and solution-assisted methods. Of these, the solvent-assisted method mainly utilizes water, inorganic acids, alkalis and organic solvents as the machining environment medium. For both simultaneous processing and postprocessing of chemical liquids, waste liquid treatment and recovery must be considered to ensure a green and pollution-free drilling process, which increases the cost of drilling. Additionally, the hole drilling strategy mostly uses percussion drilling, which is not suitable for processing large or noncircular holes. This type of research proves that the method of composite processing can improve the processing quality or efficiency, but the majority of the composite methods need to change the processing motion platform and install the unit of composite control, which increases the processing cost and is not conducive to industrial application.

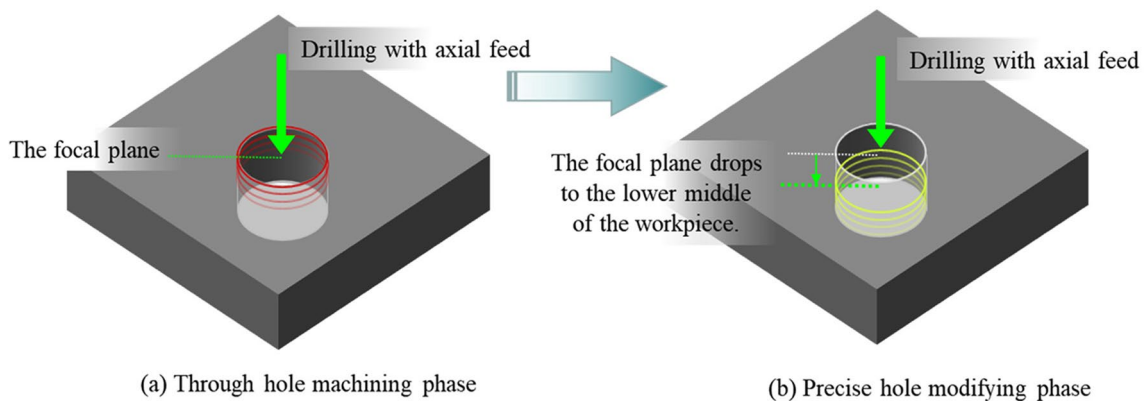
The high-efficiency and high-precision machining of air film holes still faces many challenges concerning the reliability and the consistency control. Due to the high cost of laser processing, laser-relevant process variables and their effects have always been the key to obtaining the required features and maintaining cost-effectiveness. At present, the processing strategies, the laser source and the processing methods still need researchers to innovate processing methods, improve processing techniques and develop processing equipment. Therefore, we proposed a two-step femtosecond laser drilling method with LTD [45], including the through hole machining phase and the precise hole modifying phase, and the drilling schematic diagram of the method is shown in Fig. 1. Through in situ secondary hole

**Table 1** The partial list of studies on laser-based hybrid/cross/assisted drilling techniques

Laser-based hybrid/cross/assisted drilling techniques	Laser source	Drilling material	Drilling strategy	Ref	
Ultrasonic-assisted laser drilling	Millisecond laser	Nickel superalloy GH4037	Percussion drilling	[7]	
	Millisecond laser	Chromium–nickel stainless steel 304 (SS304) sheets	Percussion drilling	[26]	
	Millisecond laser	Nickel superalloy GH4037	Single-pulse drilling	[15]	
	Femtosecond laser	Copper substrate	Percussion drilling	[27]	
Electric field assisted laser drilling	Millisecond laser	Titanium alloy TA2	Percussion drilling	[28]	
Electrochemical assisted laser drilling	Nanosecond laser	Nickel superalloy IN718	Percussion drilling	[29, 30]	
	Millisecond laser	Nickel superalloy IN718	Trepan drilling	[31]	
Solvent-assisted laser drilling	Water Waterjet	Millisecond laser	Alumina ceramics	Percussion drilling	[32]
		Nanosecond laser	Nickel-based single crystal turbine blades	Percussion drilling	[33]
	Water and methanol	Nanosecond laser	Silicon carbide	Trepanning	[34]
	Deionized water, KOH and HF solution	Femtosecond Laser	Silica	Percussion drilling	[35]
	Methanol, ethanol and isopropanol	Femtosecond Laser	Silica	Percussion drilling	[36]
	Water and additional use of ultrasonic wave agitation	Femtosecond Laser	Glass	Percussion drilling	[37]
	NaCl solution	Nanosecond laser	Stainless steel 316	Percussion drilling	[38]
	H <sub>3</sub> PO <sub>4</sub> solution	Nanosecond laser	Nitinol	Percussion drilling	[39]
	Mixed solution of HCl and NaNO <sub>3</sub>	Nanosecond laser	Nickel superalloy IN718	Percussion drilling	[40]
	Laser drilling and chemical etching (post-processing)	HF acid solution	Femtosecond Laser	Silica	Percussion drilling
Mixed solution of HF and HNO <sub>3</sub>		Femtosecond laser	Silicon carbide	Percussion drilling	[42, 43]
HF acid solution		Femtosecond laser	Photosensitive glass	Percussion drilling	[44]

reaming, the processing quality of the hole can be significantly improved while avoiding secondary errors, but the machining efficiency and laser energy utilization ratio need to be improved. Then, the following work focused in-depth research on this issue. Specifically, the influence mechanism

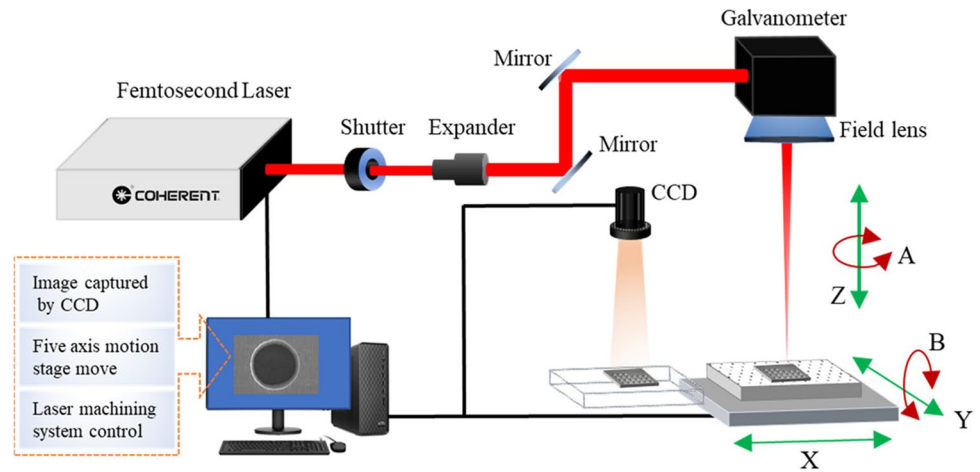
of important processing parameters (feeding times, circle numbers of nested circle scanning) on hole machining was studied, for maximizing the use of laser ablation depth and area, exploring the best processing strategy and improving efficiency while controlling the precise geometry.



**Fig. 1** The drilling schematic diagram of the two-step method

**Table 2** Chemical composition of IN792 alloy

Element	Cr	Co	Mo	W	Al	Ti	Ta	B	Zr	C	Ni
wt. %	12.4	9.2	1.9	3.9	3.5	3.9	4.2	0.016	0.018	0.07	Balance

**Fig. 2** Schematic diagram of the micromachining system

## 2 Experimental details

### 2.1 Workpiece material

The chemical composition of nickel-based superalloy IN792 used in this work is listed in Table 2. The material used was a sheet of 0.68 mm thickness and 20 mm × 20 mm in size. Holes with diameters of 0.60 mm were set to be processed in the experiments, and drilling was performed with the same machining parameter for each row to reduce error. Each row had 8 holes, and the experimental average was taken.

### 2.2 Experimental setup

The femtosecond laser micromachining system consisted of various subsystems, such as the laser source, the unit of beam delivery, the module scanning galvanometer, the monitoring system, the high-precision five-axis positioning and the motion platform. The laser used in the experiments was a femtosecond laser device (Monaco, Coherent), and the laser beam was focused on the IN792 sample surface by the field lens through the beam expander (Jenoptik, 2~10×), mirror and scanning galvanometer (Scanlab IntelliSCAN14). The schematic diagram and detailed specification of the micromachining system are shown in Fig. 2 and Table 3. As shown in Fig. 3, the laser beam rotates along the circumference of the hole, and the scanning path is nested circular scanning from inside to outside, as shown in Fig. 3 (a). Figure 3 (b) shows the surface morphology of laser processing.

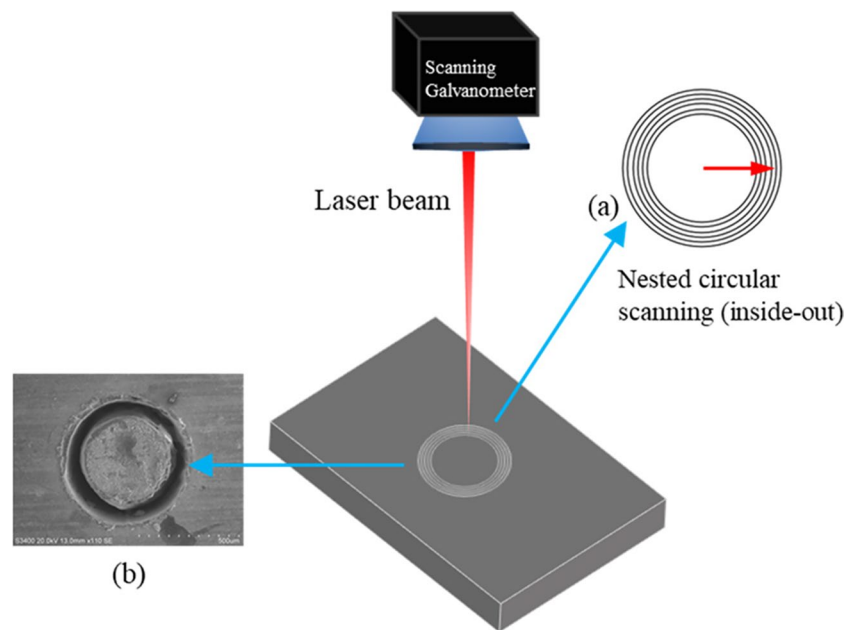
**Table 3** Specification of drilling setup

Specification	Description
Wavelength	1035 ± 5 nm
Average output power	> 40 W @ 1 MHz
Energy per pulse	> 40 μJ over entire out rep rate range
Pulse repetition rate range	Single shot to 1 MHz
Spatial mode	TEM <sub>00</sub> ( $M^2 < 1.2$ )
Pulse width	400~10 ps
Focal spot diameter	16 μm
Focal length	100 mm
Focus depth	0.1 mm
Single scanning range	45 mm × 45 mm
Scanning speed of galvanometer	≤ 3000 mm/s
Scanning accuracy of galvanometer	≤ ± 5 μm

### 2.3 Evaluation of hole quality characteristics

In the course of hole machining, the machining quality of the hole can be roughly observed by CCD in real time, which is convenient to adjust the process parameters in time. After the completion of the experiments, the microscopic views and microstructure of the cross-sectional holes were observed by means of laser scanning confocal microscopy (LSCM, VK-X1000, Keyence) and scanning electron microscopy (SEM, S-3400N, Hitachi). The hole circularity at the entrance and exit and the hole taper were measured. Hole circularity ( $HC$ ) was calculated using Eq. (1) by measuring diameters at different points and dividing the minimum

**Fig. 3** The laser trepan drilling method: (a) the scanning path and (b) the surface morphology of laser processing



diameter ( $D_{min}$ ) by the maximum diameter ( $D_{max}$ ). The taper angle ( $TA$ ) was calculated by Eq. (2), where  $T$  is the sample thickness and  $D_{entrance}$  and  $D_{exit}$  are the entrance and exit diameters, respectively:

$$HC = \frac{D_{min}}{D_{max}} \times 100\% \quad (1)$$

$$TA = \arctan \frac{D_{entrance} - D_{exit}}{2T} \quad (2)$$

### 3 Results and discussion

#### 3.1 The influence of feeding times on hole machining accuracy

To further accurately control the geometry of the machining hole and optimize the two-step machining strategy, the influence of the feeding times on the process of hole forming was studied. According to previous research results [45], hole machining was performed following a nested circular scanning path (inside-out) and with an axial feed method. The preset processing hole diameter was 0.6 mm, and the intervals between scanning lines were set to 0.01 mm. The feeding times was increased from 1 to 8, and the surface morphology and the dimensional accuracy of the hole entrance and exit were observed in detail. As shown in Fig. 4, after the first feeding (Fig. 4(a)), the depth of the blind hole was almost 0.20–0.30 mm; after the second feeding (Fig. 4(b)), the through hole formed, and the

entrance was regular and circular, but the exit was irregular; then, as feeding times increased (Fig. 4(c–h)), the hole circularity at the entrance and exit gradually increased, and the ellipticity of exit gradually decreased. The analysis and observation of the changes in the entrance diameter illustrated that the diameter linearly and directly correlated with the number of feedings; the change is shown in Fig. 5a, and the slope after linear fitting was 5.0595 (Fig. 5b). In a certain range, the change in the inlet diameter with the number of feeding can be calculated with the following equation,  $y = 5.0595x + 598.75$ , where  $x$  is the number of feeding times and  $y$  is the entrance diameter. Besides, the exit is prone to from oval shape as shown in Fig. 4(c<sub>2</sub>–h<sub>2</sub>), and the diameter changes in the long axes and short axes with the number of feeding times shown in Fig. 5 c and d. Due to scanning errors of the galvanometer and energy loss caused by constant refraction and reflection of the laser in the hole during axial feeding, differences in exit size accumulate continuously in both directions. As a result, the growth rate of the diameter of the long axis is less than that of the diameter of the short axis with the increase of the number of feeding times, and the hole circularity of the exit is continuously optimized, as shown in Fig. 4(c<sub>2</sub>–h<sub>2</sub>). According to the above analysis, the linear relationship between feeding times and entrance can provide a theoretical basis for the shape control of nickel-base superalloy drilling, but simply increasing the feeding times will make the entrance diameter deviate from the preset size gradually and increase the hole taper, so that high-quality hole machining cannot be realized. It is necessary to optimize other parameters at the same time to achieve the purpose of precise shape control.

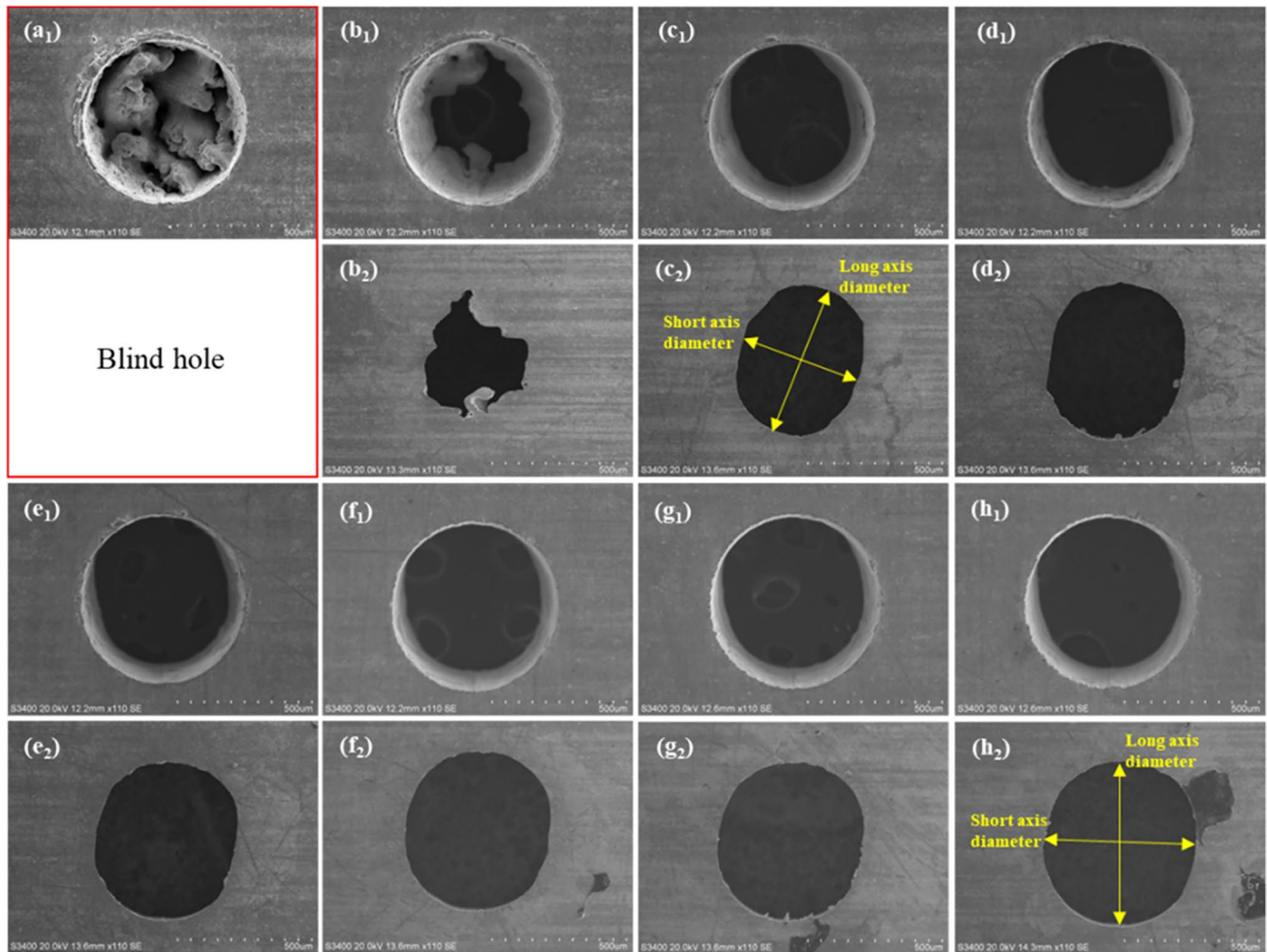


**Fig. 4** Surface morphology of the hole entrance and exit under different feeding times: (a) feeding 1 time; (b) feeding 2 times; (c) feeding 3 times, (d) feeding 4 times, (e) feeding 5 times, (f) feeding 6 times,

(g) feeding 7 times and (h) feeding 8 times. The first and third lines are the entrance, and the second and fourth lines are the corresponding morphology on the exit side of the holes

### 3.2 The influence of optimizing the circle number of nested circle on drilling efficiency

The proposed two-step method includes the through hole machining phase and the precise hole-modifying phase. In the initial research, to ensure the formation of the through hole, the initial diameter of the nested circle scanned from inside to outside was 0.02 mm and was simultaneously increased to 0.6 mm in 0.01-mm increments. Then, this femtosecond laser trepanning method with a nested circular scanning path was not only time-consuming but also had a low laser utilization rate. However, as shown in Fig. 3(b), provided that the drilling process parameters are not accurate (especially if the circle number of the nested circle is too small), the area in the middle of the hole cannot be ablated by the laser, and it consequently cannot be cut off along the circular trajectory, which prevents the formation of the through hole. In addition, in the repair stage after

the formation of the through hole, the repeated scanning of the through area that has been ablated by the laser will reduce the laser utilization rate and the processing efficiency. Therefore, accurately determining the starting circle diameter and maximizing the laser utilization rate to complete the through hole processing phase and the modifying phase are very important. As shown in Fig. 6a–h, the number of scanning circles in the nested circular scanning path was gradually reduced to improve laser processing efficiency, and the impact of this reduction on hole drilling was investigated. In addition, the preset machining diameter was 0.60 mm, and since the spot diameter was 0.016 mm, the actual ablation diameter of the hole after laser ablation was nearly 613  $\mu\text{m}$ , as shown in Fig. 6i.

According to the scanning path in Fig. 6, the entrance and exit morphology under different scanning turns was observed, as shown in Fig. 7, and the geometry profile is shown in Fig. 8. The machining scanning path (a–f) can

**Fig. 5** Variation of entrance and exit diameter with an increase of the feeding times: **a** the variation of entrance diameter, **b** the fit plot line of **a**, **c** the variation of exit diameter of short axis and **d** the variation of exit diameter of long axis

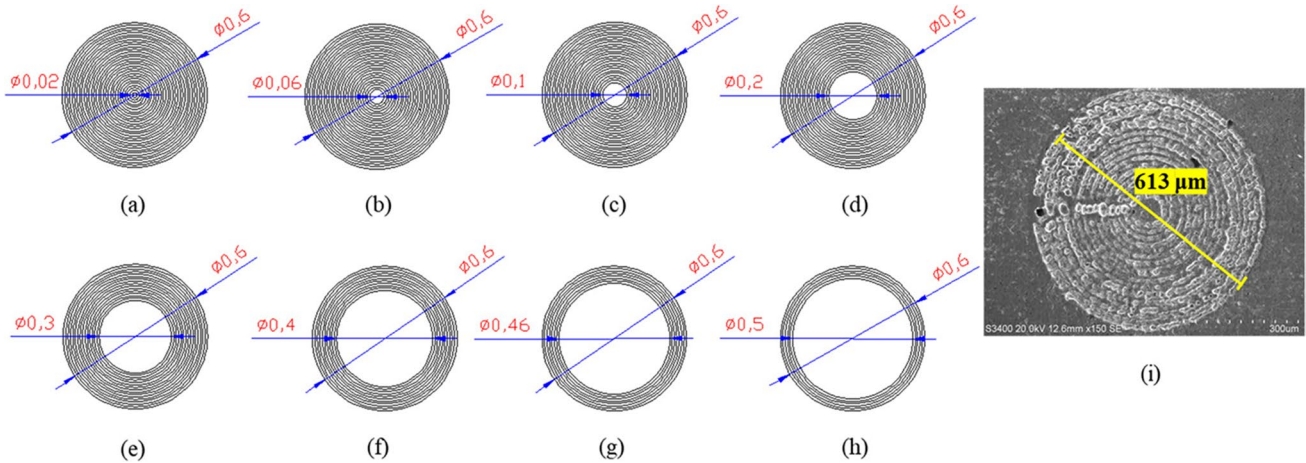
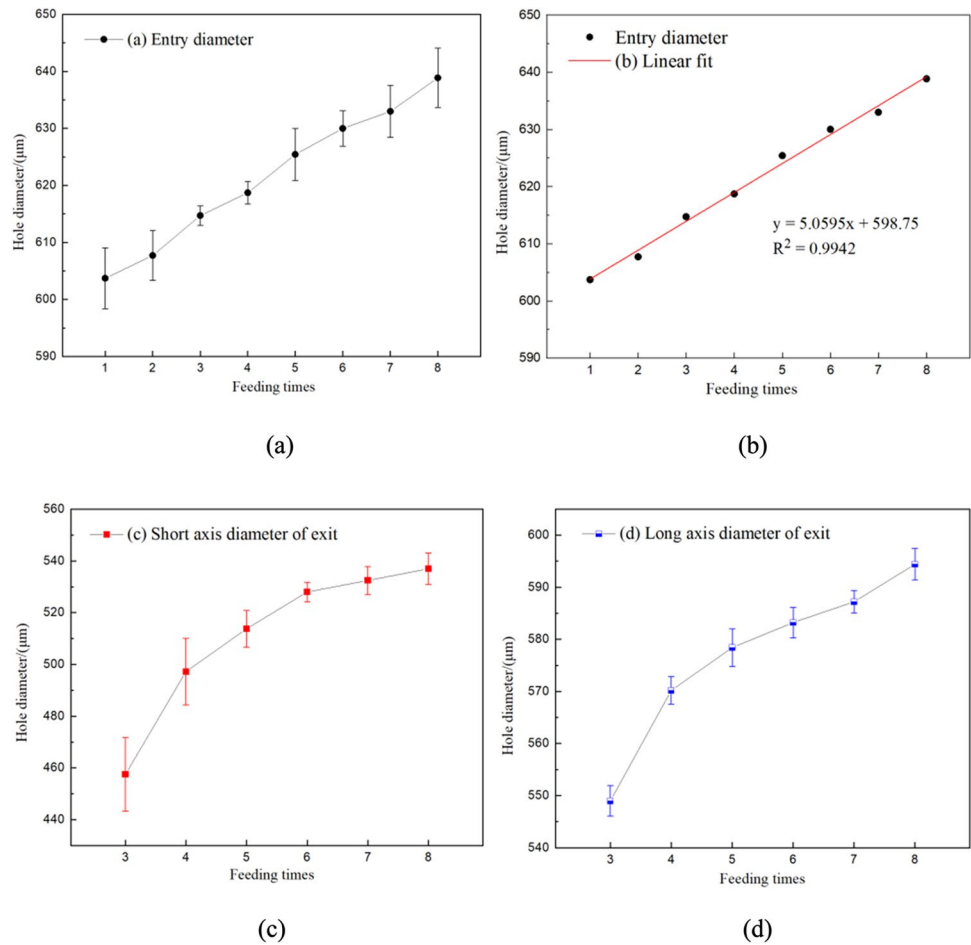


**Fig. 6** The schematic diagram of the nested circular scanning path (inside-out): **a** nesting circle diameter from 0.02 to 0.6 mm, **b** nesting circle diameter from 0.06 to 0.6 mm, **c** nesting circle diameter from 0.1 to 0.6 mm, **d** nesting circle diameter from 0.2 to 0.6 mm, **e** nest-

ing circle diameter from 0.3 to 0.6 mm, **f** nesting circle diameter from 0.4 to 0.6 mm, **g** nesting circle diameter from 0.46 to 0.6 mm, **h** nesting circle diameter from 0.5 to 0.6 mm and **i** the surface morphology of the drilling hole after one laser scanning

be processed into a through hole. When the scanning turns were not enough, such as track (g, h), the ablated material cannot be completely separated from the base material, some

unmelted materials are connected to the base material, and the through holes cannot be formed, as Figs. 7(g<sub>2</sub>, h<sub>2</sub>) and 8(g, h) show. Combining the hole morphology in Fig. 7 and

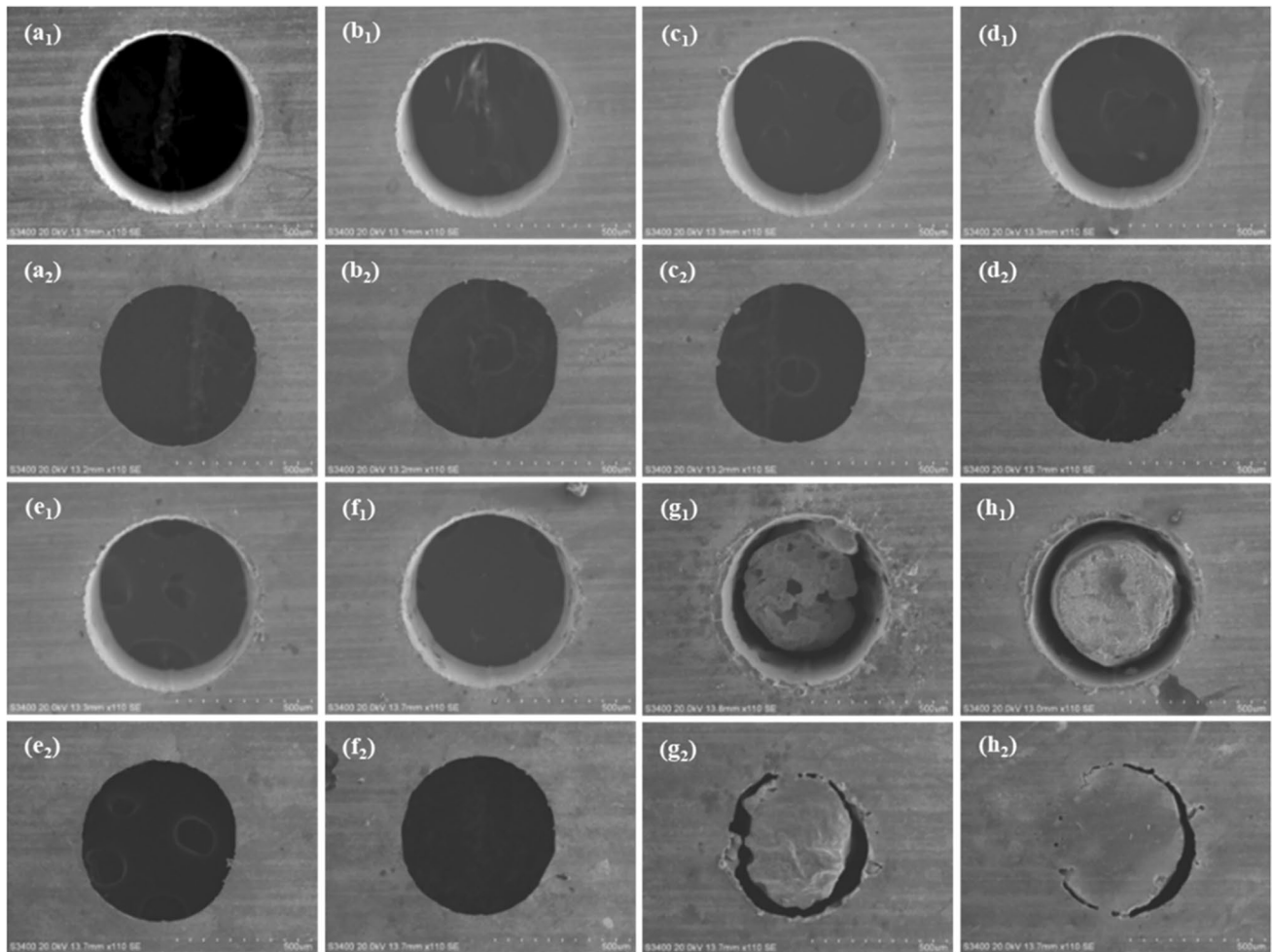


**Fig. 7** Surface morphology of entrance and exit holes processed under different nested circular scanning paths: (a) nesting circle diameter from 0.02 to 0.6 mm, (b) nesting circle diameter from 0.06 to 0.6 mm, (c) nesting circle diameter from 0.1 to 0.6 mm, (d) nesting circle diameter from 0.2 to 0.6 mm, (e) nesting circle diameter

from 0.3 to 0.6 mm, (f) nesting circle diameter from 0.4 to 0.6 mm, (g) nesting circle diameter from 0.46 to 0.6 mm and (h) nesting circle diameter from 0.5 to 0.6 mm. The first and third lines are the entrance, and the second and fourth lines are the corresponding morphology on the exit side of the holes

the hole geometry (a–f) in Fig. 8 illustrates that when the diameter of the inner circle of the trepanning circle was in the range of 0.02~0.40 mm, the impact on hole drilling was small, and the hole geometry did not markedly change. Fortunately, after reducing the number of scanning turns, the processing time markedly decreased, from 92 to 58 s, and the processing efficiency increased by 36.9%, as shown in Fig. 9. By studying the influence of the circle number on hole drilling, it can provide a theoretical basis for determining the scanning path and the circle number of the through hole machining phase and the precise hole-modifying phase. It follows that optimizing the processing technology, such as selecting the appropriate scanning path and the number of scanning turns, can significantly shorten the processing time and reduce the processing cost while ensuring the drilling quality, which is more conducive to industrial production.

These research results are not only applicable to the two-step method proposed, but also applicable to most of the trepanning process technologies.

### 3.3 Optimization of the two-step laser trepanning strategy

On the basis of previous research, the influence of feeding times and circle numbers of scanning path on hole machining has been clearly defined; this section will upgrade the two-step drilling method by adjusting the parameters that have a greater impact on the processing quality to improve the trepanning strategy and, ultimately, machining accuracy, machining efficiency and laser utilization. The technological parameters of the two-step method before optimization are shown in Table 4. A series of process optimization studies



**Fig. 8** Geometry profile of the holes processed under different nested circular scanning paths: (a) nesting circle diameter from 0.02 to 0.6 mm, (b) nesting circle diameter from 0.06 to 0.6 mm, (c) nesting circle diameter from 0.1 to 0.6 mm, (d) nesting circle diameter from 0.2 to 0.6 mm, (e) nesting circle diameter from 0.3 to 0.6 mm, (f) nesting circle diameter from 0.4 to 0.6 mm, (g) nesting circle diameter from 0.46 to 0.6 mm and (h) nesting circle diameter from 0.5 to 0.6 mm

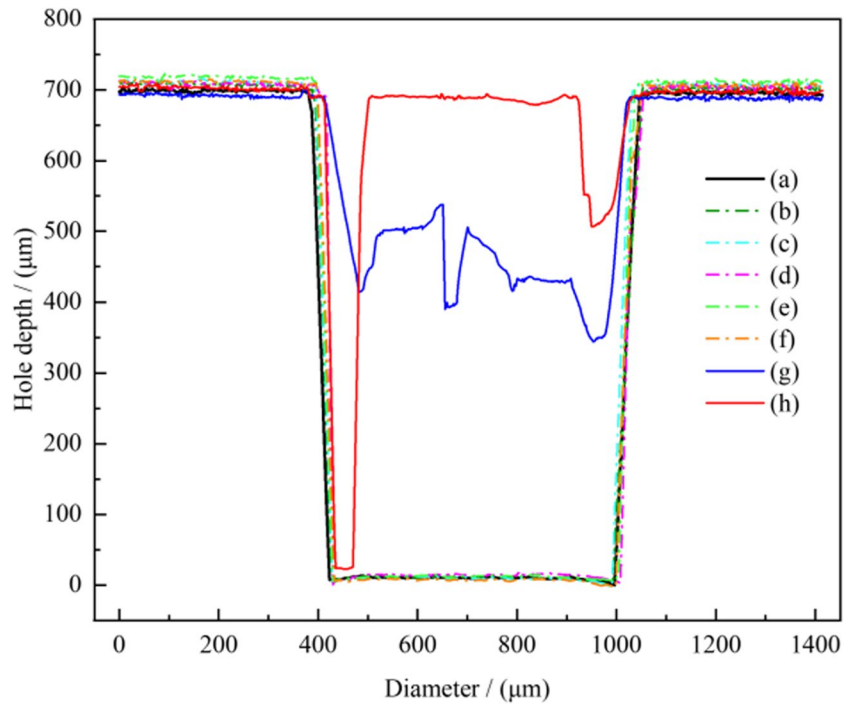
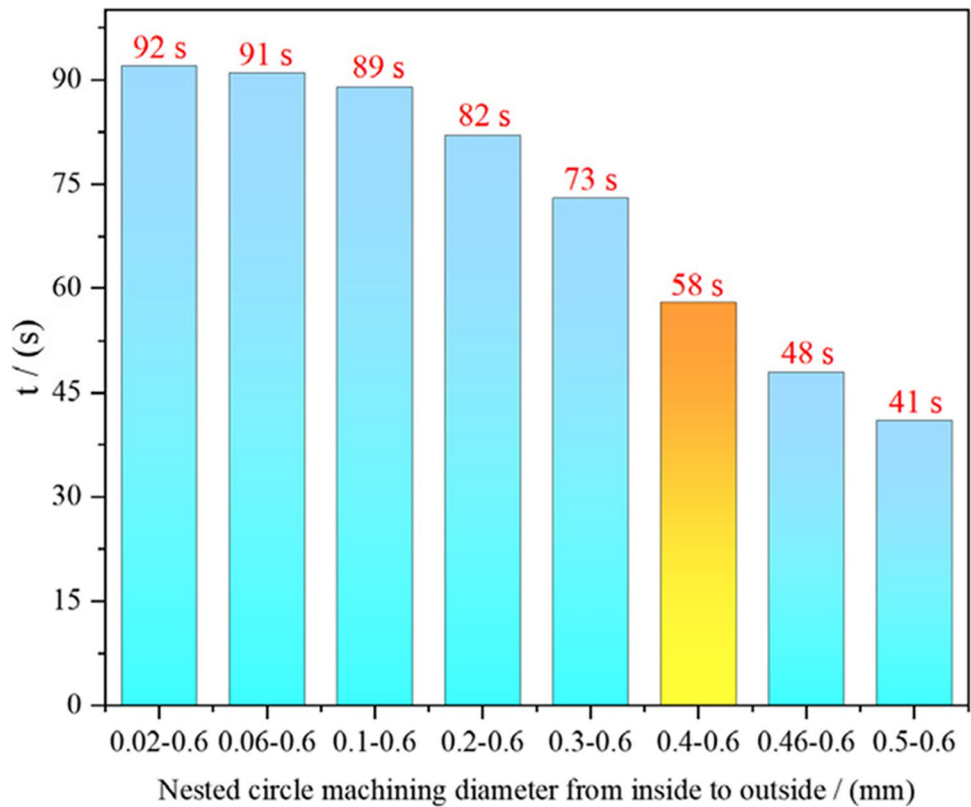


**Fig. 9** Laser drilling time under different nested circular scanning paths



yielded the important factors that affect the machining quality and precision, and some typical experiments are selected for illustration. The first step was to machine through holes followed by post-processing. In the subsequent steps, the

processing focus was lowered, and the processing accuracy of the prefabricated hole bottom was modified and improved by increasing the single-layer scanning times, reducing the number of circumscribed circles and reducing the scanning speed,

**Table 4** The processing parameters of the two-step method on 0.68 mm thick IN792 sheets before optimization

Processing parameters	Nesting scanning circle diameter (mm)	Scanning speed (mm/s)	Feeding times	Single-layer laser scanning times	Inlet circularity	Outlet circularity	taper angle (°)
Step 1	0.02~0.6	300	4	80	99.6%	98.0%	2.0–3.3
Step 2	0.02~0.6	300	4	120			

**Table 5** The hole-machining parameters and quality characteristic parameters with different processing strategies on 0.68-mm-thick IN792 sheets

Nesting scanning circle diameter (mm)	Scanning speed (mm/s)	Feeding times	Scanning times of each layer	$HC_{entrance}$ (%)	$HC_{exit}$ (%)	TA (°)	Drilling time (s)	
Strategy (a)	0.3~0.6	300	5	80	99.2%	88.1%	2.2~5.1	36
Strategy (b)	0.3~0.6	300	5	80	99.3%	98.3%	2.1–2.7	156
Strategy (c)	0.4~0.6	100	10	100	<b>99.4%</b>	<b>99.1%</b>	<b>1.6~2.3</b>	<b>112</b>
	<b>0.3~0.6</b>	<b>300</b>	<b>5</b>	<b>80</b>				
Strategy (d)	<b>0.4~0.6</b>	<b>100</b>	<b>5</b>	<b>120</b>	99.6%	98.0%	2.0~2.7	103
	0.3~0.5	300	5	80				
Strategy (e)	0.3~0.6	300	5	80	99.5%	98.8%	2.2~2.4	161
	0.4~0.6	100	5	100				
	0.4~0.6	100	5	120				

The data in bold represent the optimal processing strategy

which finally improved the laser utilization rate by optimizing the processing strategy. According to the results in “The influence of feeding times on hole machining accuracy” and “The influence of optimizing the circle number of nested circle on drilling efficiency”, the scanning path of Fig. 6e is selected for the first step of machining in order to ensure that the through hole machining and the dimensional accuracy of the hole entrance meet the expectations. After four times of feeding, the exit diameter is about 0.49~0.57 mm according to the machining results in Fig. 5c, d. Thus, the scanning path shown in Fig. 6(f) is selected to ensure the accuracy of hole modifying and the consistency of results. Moreover, the hole machining parameters and the drilling time corresponding with different strategies are shown in Table 5, and the quality characteristic parameters are also listed, which were calculated according to Eqs. (1) and (2).

Figures 10 and 11 present the geometry profile and the surface morphology of the entrance and exit holes processed under different processing strategies. Strategy (a) is the first step of the process, and the others are multistep process. The hole machining quality and accuracy were significantly improved after post-processing optimization, especially the circularity and machining size of the exit. Comparing the processing results of strategy (b) and strategy (c) found that increasing the single-layer scanning times is better than increasing the feeding times in trepan drilling, as shown in Figs. 10 and 11. In strategy (b), the single-layer scanning

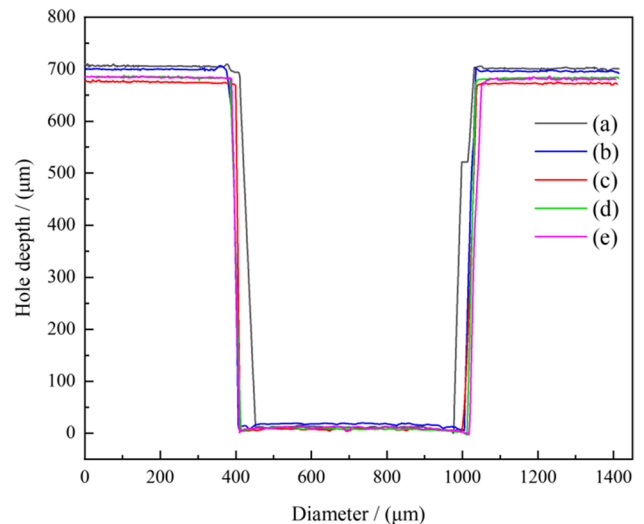


**Fig. 10** Geometry profile of the holes processed under different multistep processing strategies (corresponding to different processing strategies in Table 5): strategy (a) is the one-step process; strategies (b), (c) and (d) are the two-step processes; and strategy (e) is the three-step process

time was increased to 100, and the material still could not be completely discharged; even if the feeding times were increased, the processing effect was not as good as in strategy (c). In strategy (c), setting the laser focus at the bottom of the material and increasing the single-layer scanning

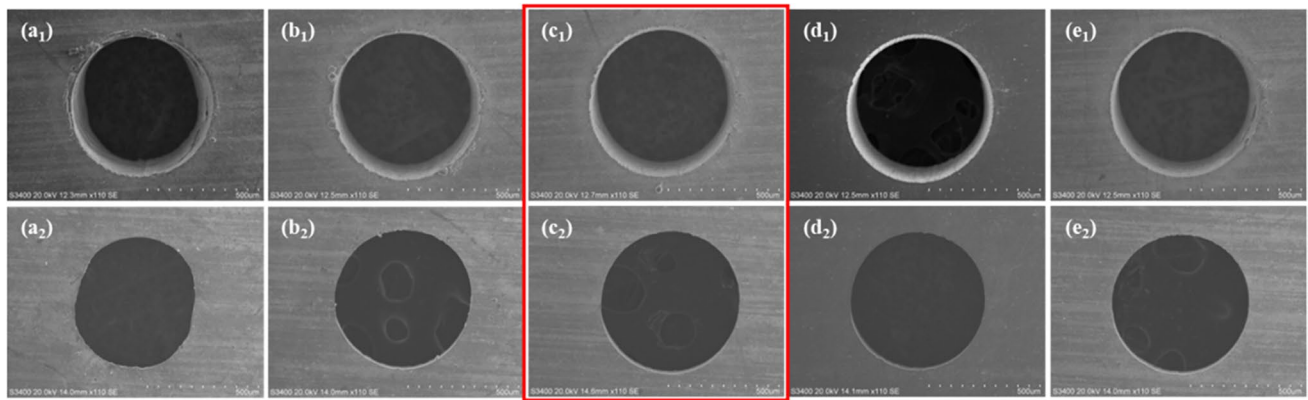


**Fig. 11** Surface morphology of the hole entrance and exit processed under different multistep processing strategies (corresponding to different processing strategies in Table 5): strategy (a) is one-step pro-

cess, strategies (b), (c) and (d) are two-step processes, and strategy (e) is a three-step process

times to 120 improved the processing effect, which is more conducive to removing material and reaming a more accurate orifice. Furthermore, to improve the utilization rate of the laser energy, strategy (d) first machining through holes with small diameters and then modify the holes. Experiments show that the exits and entrances processed with this method are smaller and not ideal, and the taper is larger than that of strategy (c), indicating that the through hole phase of the first step requires machining the entrance with preset size. The small entrance hinders the incidence of the laser and affects the hole drilling accuracy. In addition, strategy (e) is a three-step process, and the second and third steps are both the modifying phase. The experimental results show that although two-step reaming can improve the circularity of the entrance and exit, excessive repeated ablation will continue to expand the hole, resulting in an increase in the hole taper, and the processing effect is also not as good as that of strategy (c). In this experiment, strategy (c) was the optimal processing technology. Compared to the two-step process before optimization in Table 4, fewer scanning turns (with a diameter of 0.3~0.6 mm, 0.4~0.6 mm) were used to improve the processing efficiency (112 s), and increasing the scanning times of a single layer optimized the machining quality and accuracy of the lower part of the holes to the maximum extent and achieved the expected effect. Therefore, according to the thickness of the processing materials, moderately increasing the single-layer scanning and feeding times to find the appropriate modifying technology is the key to improving machining quality and machining accuracy.

### 3.4 Effect of laser ablation on base material characteristics in drilling process

During the infrared laser drilling process, the material is removed by hot melting to form holes. At the same time,

the instantaneous high energy and heat will have a thermal influence on the base material, resulting in defects, such as recast layers, HAZ, microcrack and oxide layers. In order to verify the high-quality machining characteristics of two-step drilling, SEM was used to characterize the orifice morphology of femtosecond laser-processed blind holes and through holes; spot scanning of the EDS method was used to analyse the main elements and atomic percentages in different regions. At the same time, the line scanning method was used to characterize the line distribution of element content in the direction from the orifice to the base material. First, spot scanning was performed on the interior of the blind hole and surface of the base material, and the EDS results are shown in Fig. 12. Figure 12 (a<sub>1</sub>) is the main element composition content map of point A that represents the base material, and Fig. 12(a<sub>2</sub>) is the main element composition content map of point B that represents ablative products that have not been discharged in time from the blind hole. Analysing the content changes of the main elements Ni, Cr, Fe and O shown that the oxygen content in the incompletely removed part of the hole increased by approximately 22% compared with the base material, which further verified that the femtosecond laser trepanning removes material by oxidative ablation. In the line scanning result of Fig. 12(a<sub>3</sub>), the oxygen content gradually decreased from the orifice to the base material, indicating that the oxidation zone of femtosecond laser processing was very small, only a few microns. In addition, a line-scanning test was also performed on the orifice of the through hole extending to the base material, which also showed that the oxygen content was essentially constant (Fig. 12(b<sub>1</sub>)). The generation of material oxides is the main source of oxygen. To further analyse the thermal influence on the base material inside the hole wall, the hole was cut sideways, and the hole cross section was observed in detail by SEM. As Fig. 13 shows, HAZ and microcrack

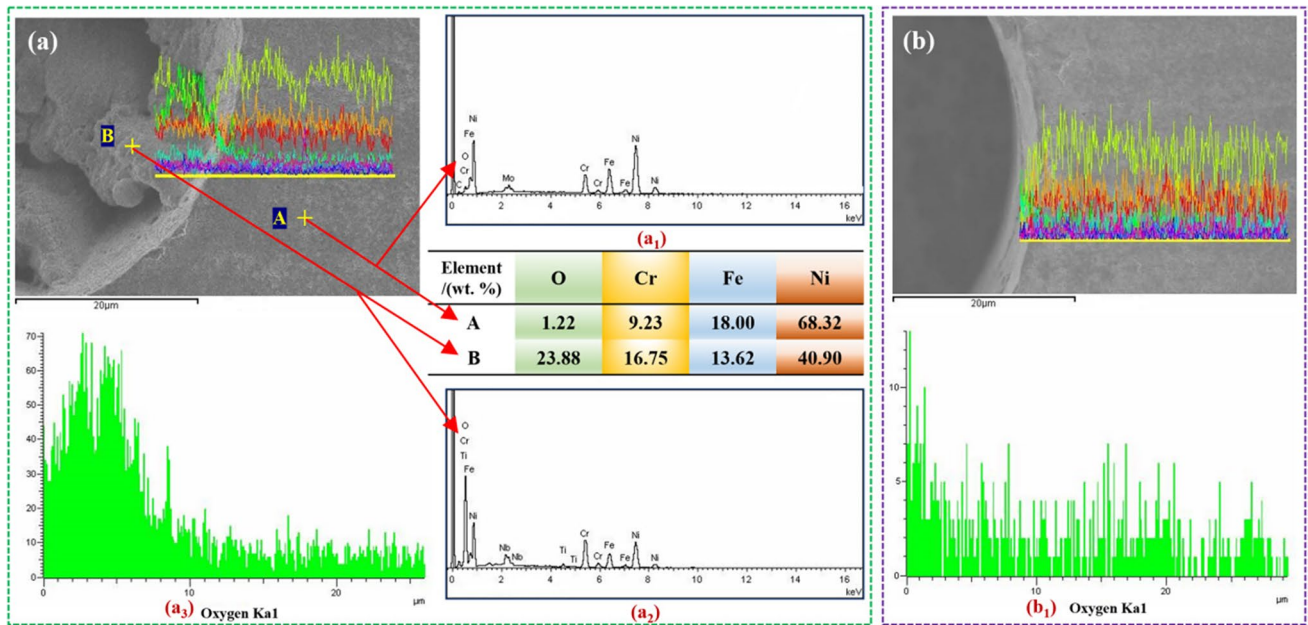


**Fig. 12** SEM morphology and composition distribution of the blind and through holes: (a) SEM image of the blind hole, (a<sub>1</sub>) composition distribution of the selected point of A, (a<sub>2</sub>) composition distribution

of the selected point of B, (a<sub>3</sub>) composition distribution curve of the selected line in (a); (b) SEM image of the through hole and (b<sub>1</sub>) composition distribution curve of the selected line in (b)

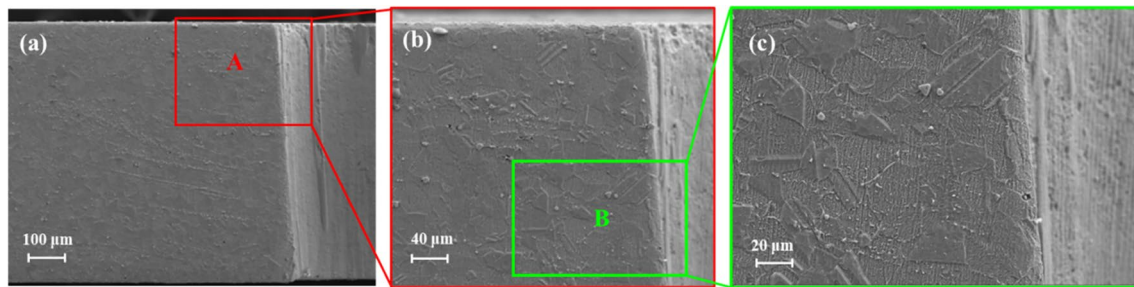


**Fig. 13** SEM morphology and the partially enlarged view of the hole cross section: (a) the hole cross section, (b) enlarged view of area A and (c) enlarged view of area B

were not evident on the hole wall when magnified in regions A and B, respectively. No debris or recast accumulation was found at the orifice, and the hole wall and the orifice processing surface were relatively flat and smooth. The data show that this femtosecond laser two-step method can machine holes with high surface quality and almost no HAZ, oxidation zone or recast layer.

## 4 Conclusions

In the present study, FCHs of nickel-base superalloys were drilled by a 1035-nm femtosecond laser in trepanning with optimization of the drilling strategy. The optimum results prove the considerable improvements in the hole geometrical characteristics at the laser beam entrance and

exit sides, and the machining efficiency was also greatly improved. The following conclusions were drawn from the experimental investigation:

The feeding times linearly correlated with the entrance diameter as follows:  $y = 5.0595x + 598.75$ , which can provide a reference for the precise geometry control of nickel-based superalloy drilling.

Optimizing the processing technology and choosing the appropriate scanning path and number of scanning turns can significantly shorten the processing time and reduce the processing cost while ensuring the drilling quality. When the trepanning circle is in the range of 0.40–0.60 mm, the processing time is greatly shortened, and the processing efficiency is increased by 36.9%.

Referring to the above two conclusions has important guiding significance for formulating the machining parameters of two-step process. In addition, increasing the single-layer scanning times is better than increasing the feeding times in trepan drilling; the modifying process can improve the circularity, but excessive repeated ablation will continue to expand the hole, resulting in a decrease in the hole taper.

This femtosecond laser two-step method can machine holes with high surface quality and almost no HAZ, oxidation zone or recast layer.

In conclusion, this research further studied how to improve the hole geometrical characteristics and machining efficiency, provides a technical reference for the two-step method of high quality drilling and improves the axially symmetrical geometry of the hole for deep drilling process.

**Author contribution** Fengyun Zhang: methodology, data curation, writing original draft. Shufeng Sun: resources, funding acquisition, supervision, project administration. Xi Wang: formal analysis, validation. Jin Wang: validation, data curation. Yong Pang: conceptualization, formal analysis. Jian Zhang: investigation. Jing Shao: investigation, visualization.

**Funding** This work was supported by 111 project of China [No. D21017]; Belt and Road Innovative Talents Exchange Program, China [No. DL2021025003L]; Major Science and Technology Innovation project of Shandong Province [No. 2019JZZY010402]; Science and Technology Project of Qingdao West Coast New Area [No. 2021–70]; China Postdoctoral Science Foundation [No. 2020M672016].

**Data availability** All data generated or analysed during this study are included in this published article.

## Declarations

**Ethical approval** All the authors confirm that they follow all ethical guidelines.

**Consent to participate** The authors declare that they consent to participate in this paper.

**Consent for publication** The authors declare that they consent to publish this paper and agree with the publication.

**Competing interests** The authors declare no competing interests.

## References

- Panigrahi D, Rout S, Tripathy SS, Patel SK, Dhupal D (2021) Optimization and simulation of laser beam trepanning approach on DSS superalloy. *Mater Today: Proc* 44:1916–1924. <https://doi.org/10.1016/j.matpr.2020.12.094>
- Ghoreishi M, Nakhjavani OB (2008) Optimisation of effective factors in geometrical specifications of laser percussion drilled holes. *J Mater Process Technol* 196:303–310
- Meijer J (2004) Laser beam machining (LBM) state of the art and new opportunities. *J Mater Process Technol* 149(1–3):2–17. <https://doi.org/10.1016/j.jmatprotec.2004.02.003>
- Dubey AK, Yadava V (2008) Experimental study of Nd:YAG laser beam machining—an overview. *J Mater Process Technol* 195(1–3):15–26. <https://doi.org/10.1016/j.jmatprotec.2007.05.041>
- Dubey AK, Yadava V (2008) Laser beam machining—an review. *Int J Mach Tools Manuf* 48(6):609–628. <https://doi.org/10.1016/j.ijmactools.2007.10.017>
- Bandyopadhyay S, Gokhale H, Sarin Sundar JK, Sundararajan G, Joshi SV (2005) A statistical approach to determine process parameter impact in Nd:YAG laser drilling of IN718 and Ti-6Al-4V sheets. *Opt Lasers Eng* 43(2):163–182. <https://doi.org/10.1016/j.optlaseng.2004.06.013>
- Xia K, Wang H, Ren N, Ren X, Liu D, Shi C, Li T, Tian J (2021) Laser drilling in nickel super-alloy sheets with and without ultrasonic assistance characterized by transient in-process detection with indirect characterization after hole-drilling. *Opt Laser Technol* 134:106559. <https://doi.org/10.1016/j.optlastec.2020.106559>
- Zhang Y, He X, Yu G, Li S, Tian C, Ning W, Zhang Y (2022) Dynamic evolution of keyhole during multi-pulse drilling with a millisecond laser on 304 stainless steel. *Opt Laser Technol* 152:108151. <https://doi.org/10.1016/j.optlastec.2022.108151>
- Zhao W, Yu Z (2018) Self-cleaning effect in high quality percussion ablating of cooling hole by picosecond ultra-short pulse laser. *Opt Lasers Eng* 105:125–131. <https://doi.org/10.1016/j.optlaseng.2018.01.011>
- Saini SK, Dubey AK, Upadhyay BN, Choubey A (2018) Study of hole characteristics in laser trepan drilling of ZTA. *Opt Laser Technol* 103:330–339. <https://doi.org/10.1016/j.optlastec.2018.01.052>
- Sezer HK, Li L, Schmidt M, Pinkerton AJ, Anderson B, Williams P (2006) Effect of beam angle on HAZ, recast and oxide layer characteristics in laser drilling of TBC nickel superalloys. *Int J Mach Tools Manuf* 46(15):1972–1982. <https://doi.org/10.1016/j.ijmactools.2006.01.010>
- Wang R, Dong X, Wang K, Sun X, Fan Z, Duan W (2019) Two-step approach to improving the quality of laser micro-hole drilling on thermal barrier coated nickel base alloys. *Opt Lasers Eng* 121:406–415. <https://doi.org/10.1016/j.optlaseng.2019.05.002>
- Zhao W, Mei X, Wang L (2022) Competitive mechanism of laser energy and pulses on holes ablation by femtosecond laser percussion drilling on AlN ceramics. *Ceram Int*. <https://doi.org/10.1016/j.ceramint.2022.08.189> Accessed 22 August 2022
- Marimuthu S, Antar M, Dunleavey J (2019) Characteristics of micro-hole formation during fibre laser drilling of aerospace superalloy. *Precis Eng* 55:339–348. <https://doi.org/10.1016/j.precisioneng.2018.10.002>
- Yu Z, Hu J, Li K (2019) Investigating the multiple-pulse drilling on titanium alloy in picosecond laser. *J Mater Process Technol* 268:10–17. <https://doi.org/10.1016/j.jmatprotec.2018.12.027>
- Xia K, Ren N, Wang H, Shi C (2018) Analysis for effects of ultrasonic power on ultrasonic vibration-assisted single-pulse laser drilling. *Opt Lasers Eng* 110:279–287. <https://doi.org/10.1016/j.optlaseng.2018.04.022>
- Döring S, Richter S, Heisler F, Ullsperger T, Tünnermann A, Nolte S (2013) Influence of ambient pressure on the hole formation in laser deep drilling. *Appl Phys A* 112(3):623–629. <https://doi.org/10.1007/s00339-013-7836-7>
- Zhang Z, Liu S, Zhang Y, Wang C, Zhang S, Yang Z, Xu W (2022) Optimization of low-power femtosecond laser trepan drilling by machine learning and a high-throughput multi-objective genetic algorithm. *Opt Laser Technol* 148:107688. <https://doi.org/10.1016/j.optlastec.2021.107688>
- Lin CH, Rao ZH, Jiang L, Tsai WJ, Wu PH, Chien CW, Tsai HL (2010) Enhancement of ablation efficiency by a femto/

- nano-second dual-beam micromachining system. Proc of SPIE 7585 <https://doi.org/10.1117/12.842733>
20. Ito Y, Yoshizaki R, Miyamoto N, Sugita N (2018) Ultrafast and precision drilling of glass by selective absorption of fiber-laser pulse into femtosecond-laser-induced filament. Appl Phys Lett 113(6):061101. <https://doi.org/10.1063/1.5027421>
  21. Jia X, Chen Y, Wang H, Zhu G, Zhu X (2020) Experimental study on nanosecond-millisecond combined pulse laser drilling of alumina ceramic with different spot sizes. Opt Laser Technol 130:106351. <https://doi.org/10.1016/j.optlastec.2020.106351>
  22. Jia X, Zhang Y, Chen Y, Wang H, Zhu G, Zhu X (2019) Combined pulsed laser drilling of metal by continuous wave laser and nanosecond pulse train. Internatl J Adv Manufact Technol 104:1269–1274. <https://doi.org/10.1007/s00170-019-04139-6>
  23. Qin Y, Förster DJ, Weber R, Graf T, Yang S (2019) Numerical study of the dynamics of the hole formation during drilling with combined ms and ns laser pulses. Opt Laser Technol 112:8–19. <https://doi.org/10.1016/j.optlastec.2018.10.057>
  24. Sorgato M, Zanini F, Bertolini R, Ghiotti A, Bruschi S (2020) Improvement of micro-hole precision by ultrasound-assisted drilling of laser powder bed fused Ti6Al4V titanium alloy. Precis Eng 66:31–41. <https://doi.org/10.1016/j.precisioneng.2020.06.014>
  25. Zhang H, Di J, Zhou M, Yan Y, Wang R (2015) An investigation on the hole quality during picosecond laser helical drilling of stainless steel 304. Appl Phys A 119(2):745–752. <https://doi.org/10.1007/s00339-015-9023-5>
  26. Wang H, Dai X, Xu Y, Liu J, Shan J, Ren N, Ren X (2021) Real-time observation with metallurgical examination for laser percussion drilling in stainless steel sheets using simultaneous magnetic-ultrasonic assistance. Opt Commun 493:126869. <https://doi.org/10.1016/j.optcom.2021.126869>
  27. Park JK, Yoon JW, Kang MC, Cho SH (2012) Surface effects of hybrid vibration-assisted femtosecond laser system for micro-hole drilling of copper substrate. Trans Nonferrous Met Soc China 22:801–807. [https://doi.org/10.1016/S1003-6326\(12\)61807-X](https://doi.org/10.1016/S1003-6326(12)61807-X)
  28. Wang H, Liu J, Xu Y, Wang X, Ren N, Ren X, Hu Q (2021) Experimental characterization and real-time monitoring for laser percussion drilling in titanium alloy using transverse electric field assistance and/or lateral air blowing. J Manuf Process 62:845–858. <https://doi.org/10.1016/j.jmapro.2020.12.051>
  29. Saxena KK, Qian J, Reynaerts D (2020) Development and investigations on a hybrid tooling concept for coaxial and concurrent application of electrochemical and laser micromachining processes. Precis Eng 65:171–184. <https://doi.org/10.1016/j.precisioneng.2020.05.014>
  30. Saxena KK, Qian J, Reynaerts D (2020) A tool-based hybrid laser-electrochemical micromachining process: experimental investigations and synergistic effects. Int J Mach Tools Manuf 155:103569. <https://doi.org/10.1016/j.ijmactools.2020.103569>
  31. Duan W, Mei X, Fan Z, Li J, Wang K, Zhang Y (2020) Electrochemical corrosion assisted laser drilling of micro-hole without recast layer. Optik 202:163577. <https://doi.org/10.1016/j.ijleo.2019.163577>
  32. Li G, Shi D, Hu S, Ma C, He D, Yao K (2021) Research on the mechanism of laser drilling alumina ceramics in shallow water. Internatl J Adv Manufact Technol 118:3631–3639. <https://doi.org/10.1007/s00170-021-08190-0>
  33. Liu YZ (2020) Coaxial waterjet-assisted laser drilling of film cooling holes in turbine blades. Int J Mach Tools Manuf 150:103510. <https://doi.org/10.1016/j.ijmactools.2019.103510>
  34. Wee LM, Khoong LE, Tan CW, Lim GC (2011) Solvent-assisted laser drilling of silicon carbide. Int J Appl Ceram Technol 8(6):1263–1276. <https://doi.org/10.1111/j.1744-7402.2010.02575.x>
  35. CaoXW CQD, Fan H, Zhang L, Juodkakis S, Sun HB (2018) Liquid-assisted femtosecond laser precision-machining of silica. Nanomaterials 8(5):287. <https://doi.org/10.3390/nano8050287>
  36. Jiao LS, Ng EYK, Wee LM, Zheng HY (2011) The effect of assist liquid on the hole taper improvement in femtosecond laser percussion drilling. Phys Procedia 19:426–430. <https://doi.org/10.1016/j.phpro.2011.06.187>
  37. Hwang DJ, Choi TY, Grigoropoulos CP (2004) Liquid-assisted femtosecond laser drilling of straight and three-dimensional microchannels in glass. Appl Phys A 79(3):605–612. <https://doi.org/10.1007/s00339-004-2547-8>
  38. Li L, Achara C (2004) Chemical assisted laser machining for the minimisation of recast and heat affected zone. CIRP Ann 53(1):175–178. [https://doi.org/10.1016/S0007-8506\(07\)60672-6](https://doi.org/10.1016/S0007-8506(07)60672-6)
  39. Stephen A (2011) Mechanisms and applications of laser chemical machining. Phys Procedia 12:261–267. <https://doi.org/10.1016/j.phpro.2011.03.132>
  40. Zhang Q, Sun SF, Zhang FY, Wang J, Lv QQ, Shao Y, Liu QY, Shao J, Liu XF, Zhang Y (2019) A study on film hole drilling of IN718 superalloy via laser machining combined with high temperature chemical etching. Internatl J Adv Manufact Technol 106(1–2):155–162. <https://doi.org/10.1007/s00170-019-04541-0>
  41. Gao B, Chen T, Chen Y, Si JH, Hou X (2015) Fabrication of through micro-hole arrays in silicon using femtosecond laser irradiation and selective chemical etching. Chin Phys Lett 32(10):107901. <https://doi.org/10.1088/0256-307X/32/10/107901>
  42. Khuat V, Ma Y, Si J, Chen T, Chen F, Hou X (2014) Fabrication of through holes in silicon carbide using femtosecond laser irradiation and acid etching. Appl Surf Sci 289:529–532. <https://doi.org/10.1016/j.apsusc.2013.11.030>
  43. Khuat V, Chen T, Gao B, Si J, Ma Y, Hou X (2014) Uniform nano-ripples on the sidewall of silicon carbide micro-hole fabricated by femtosecond laser irradiation and acid etching. Appl Phys Lett 104(24):241907. <https://doi.org/10.1063/1.4883880>
  44. Wu YZ, Jia W, Wang CY, Hu ML, Ni XC, Chai L (2008) Micro-hole fabricated inside FOTURAN glass using femtosecond laser writing and chemical etching. Opt Quantum Electron 39(14):1223–1229. <https://doi.org/10.1007/s11082-008-9192-y>
  45. Zhang FY, Wang J, Wang X, Zhang J, Hayasaki Y, Kim D, Sun SF (2021) Experimental study of nickel-based superalloy IN792 with femtosecond laser drilling method. Opt Laser Technol 143:107335. <https://doi.org/10.1016/j.optlastec.2021.107335>

**Publisher's note** Springer Nature remains neutral with regard to jurisdictional claims in published maps and institutional affiliations.

Springer Nature or its licensor (e.g. a society or other partner) holds exclusive rights to this article under a publishing agreement with the author(s) or other rightsholder(s); author self-archiving of the accepted manuscript version of this article is solely governed by the terms of such publishing agreement and applicable law.